

Ultrathin CIGSe Solar Cells with Integrated Structured Back Reflector

Thomas Schneider,* Johanna Tröndle, Bodo Fuhrmann, Frank Syrowatka, Alexander Sprafke, and Roland Scheer

To reduce the thickness of $\text{CuIn}_{1-x}\text{Ga}_x\text{Se}_2$ (CIGSe) solar cells, light management concepts must be used. One concept is the combination of an Al/indium-tin-oxide (ITO) reflector/contact and an optical scattering element at the back side of the device. Herein, nanostructured substrates, obtained by laser interference lithography and lift-off process, are covered with an Al/ITO back contact. Structure dimensions are a pitch of $1.96\ \mu\text{m}$ and heights of $100\text{--}700\ \text{nm}$. Solar cells with $600\ \text{nm}$ CIGSe absorber having this integrated structured back reflector exhibit an increase in J_{SC} of up to $3.2\ \text{mA cm}^{-2}$ compared with the Mo reference sample of identical thickness. To understand this optical gain, 3D finite-difference time-domain (FDTD) simulations are performed. To this end, a model is built to simulate structure formation. It is shown that locally enhanced optical absorption can be achieved by the integrated structured back reflector. It is also shown that parasitic absorption in the back ITO diffusion barrier needs to be minimized.

1. Introduction


Reducing the thickness of thin-film solar cells reduces the total cost of ownership of solar module production. Theoretically, a $500\ \text{nm}$ $\text{Cu}(\text{In,Ga})\text{Se}_2$ (CIGSe) solar cell allows more than 20% efficiency.^[1–4] However, this requires a very low back contact recombination velocity and advanced optical light management. The standard molybdenum back contact is generally attributed with a high recombination velocity^[5–7] and has a poor optical reflectivity.^[8] In ref. [9], a ZrN layer on top of molybdenum having a reflectivity of 60% was used with the result of increased quantum efficiency at long wavelengths. An even

higher reflectivity and higher gain in photocurrent could be achieved by an Au back reflector applied by post-deposition recontacting after removing the Mo layer.^[10] In addition to cost aspects, Au is not suitable for direct deposition of CIGSe thin films at high temperatures due to the chemical reactivity with the chalcogen species during CIGSe deposition. The latter is also true for other highly reflective metals such as Ag, Cu, and Al.^[11] Instead, these metals have to be encapsulated by a transparent and conductive diffusion barrier layer. Bissig et al. investigated an Al/InZnO back contact for solar cells with an absorber thickness of $2.1\ \mu\text{m}$ and were able to increase the short-circuit density up to $1.4\ \text{mA cm}^{-2}$ compared with a sample with Mo back contact, despite the relatively high

absorber thickness.^[12] According to former work on transparent back contacts, the transparent conductor indium-tin-oxide (ITO) is a good candidate as a transparent back contact^[13] and as a diffusion barrier.^[14] Recently, ref. [15] showed an experimental gain in short-circuit current density of $4.9\ \text{mA cm}^{-2}$ in a structure Mo/Ag/ITO/ $0.5\ \mu\text{m}$ CIGSe with respect to the reference structure of Mo/ $0.5\ \mu\text{m}$ CIGSe. Al/ITO-based solar cells can be prepared up to at least $600\ ^\circ\text{C}$ without Al diffusion inside the absorber while providing high reflectivity at long optical wavelengths.^[16] This raises the question of the electronic properties of the ITO/CIGSe contact. Keller et al. investigated $650\ \text{nm}$ CIGSe bifacial solar cells with a hydrogen-doped In_2O_3 back contact^[17] and quantified the back-contact recombination velocity to the range of $10^7\ \text{cm s}^{-1}$. This value dropped by application of an $\text{Al}_2\text{O}_3 + \text{NaF}$ precursor layer stack as confirmed by a strongly increased rear-side external quantum efficiency (EQE) at short wavelengths. Unfortunately, the $5\ \text{nm}$ Al_2O_3 conformal layer reduces the fill factor (FF).^[17] Although a flat optical reflector enhances the long-wavelength EQE upon front-side illumination to some extent, light scattering is required in addition to approach the Yablonovitch limit.^[18] Yin et al. used ITO as transparent back contact and applied both dielectric SiO_2 nanoparticles on top of ITO and an external Ag mirror behind the substrate glass achieving a very high short-circuit current density of $32.4\ \text{mA cm}^{-2}$ with an absorber thickness of only $390\ \text{nm}$.^[19] This was an important step toward a structured and reflecting back contact for CIGSe solar cells. Kovacic et al. performed optical simulations with a $500\ \text{nm}$ absorber in a complete solar module stack with different back-contact metals in combination with

T. Schneider, J. Tröndle, Dr. A. Sprafke, Prof. R. Scheer
Martin-Luther-University Halle-Wittenberg
Institute of Physics
Von-Danckelmann-Platz 3, 06120 Halle (Saale), Germany
E-mail: thomas.schneider@physik.uni-halle.de

Dr. B. Fuhrmann, F. Syrowatka
Interdisziplinäres Zentrum für Materialwissenschaften (IZM)
Martin-Luther-University Halle-Wittenberg
Heinrich-Damerow Straße 4, 06120 Halle (Saale), Germany

 The ORCID identification number(s) for the author(s) of this article can be found under <https://doi.org/10.1002/solr.202000295>.

© 2020 The Authors. Published by Wiley-VCH GmbH. This is an open access article under the terms of the Creative Commons Attribution License, which permits use, distribution and reproduction in any medium, provided the original work is properly cited.

DOI: 10.1002/solr.202000295

an internal and external structure.^[20] The results show that solar cells with a 500 nm CIGSe absorber can even surpass the J_{SC} value of a standard Mo-based CIGSe solar cell with a 1800 nm thick absorber layer. Al_2O_3 was used in the simulations as diffusion barrier for the back-contact metals. For real devices, however, a different configuration has to be used because the Al_2O_3 is electrically isolating and local openings or thinning of the Al_2O_3 would compromise its diffusion barrier properties.

In this article, the functionalities of optical scattering, optical reflectivity, and electric conductivity of the back contact are fully integrated into the solar cell stack using a structured Al/ITO rear contact. The CIGSe thickness was chosen to be 600 nm as this thickness prevents pin-holes (in contrast to thinner CIGSe) but renders the back contact highly critical in terms of absorption and recombination (in contrast to thicker CIGSe). The growth of CIGSe on the nanostructured back contact is investigated, the solar cell parameters for different structure heights are determined, and optical simulations are carried out.

2. Experimental Section

Figure 1 gives a principle sketch of the applied thin-film structure. Commercial coated soda-lime glasses with 500 nm Mo layers on top of a SiO_xN_y diffusion barrier layer were used for all samples as substrate. SiO_2 nanostructures are formed by photolithography using lift-off technology. The lift-off approach was selected due to higher reproducibility. For this purpose, a negative photo-resist (AR N4240 with diluter AR 300:12 from Allresist) is deposited by spin-coating. The photoresist is illuminated by Fresnel-type laser interference lithography, baked, and developed (AR 300:475). This leads to pillar-like structures of photoresist on a hexagonal lattice. SiO_2 layers of varying thickness are deposited by e-beam deposition. Lift-off is carried out in acetone at 50 °C for 30 min in an ultrasound bath. The results are hexagonally ordered holes in SiO_2 of variable shape and size with a pitch of 1.96 μm . Structures with 197, 550, and 700 nm SiO_2 thicknesses can be seen in the upper row of **Figure 2** showing scanning electron microscopy (SEM) images.

Two sample sets were fabricated with roughly the same structural dimensions. The structure heights are 101, 197, 282, 550,

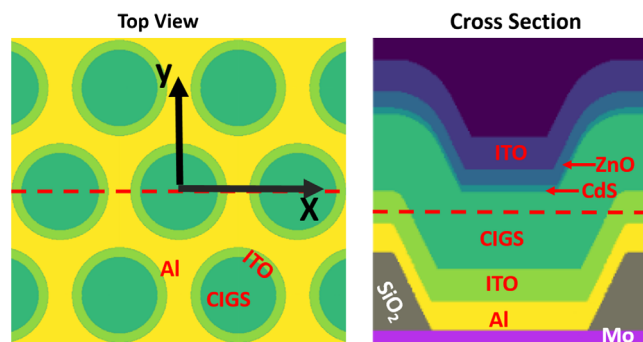


Figure 1. Schematics of the prepared solar cell with SiO_2 structure elements, aluminum metal reflector, and ITO transparent back contact underneath an ultrathin CIGSe solar cell with 0.6 μm CIGSe layer. The red dashed lines in the left picture show the axis of the right cross-section picture and vice versa.

and 700 nm for sample set 1 and 100, 174, 296, and 499 nm for sample set 2 as determined by spectral ellipsometry measurements on unstructured SiO_2 layers deposited in the same preparation processes. An aluminum layer of 110 nm thickness was deposited on top of the SiO_2 nanostructures using e-beam evaporation followed by 250 nm ITO sputtering. CIGSe layers were grown simultaneously on each sample set using the three-stage deposition process resulting in 600 nm thick layers. The chemical composition is $GGI = [Ga]/([In] + [Ga])$ of 0.37 for the first set of samples and 0.3 for the second set. The $CGI = [Cu]/([In] + [Ga])$ is 0.84 for both sample sets as determined using energy-dispersive X-ray spectroscopy measurements. The GGI depth profile was determined using Glow Discharge Optical Emission Spectroscopy (GDOES) with a commercial GDA 750 of Spectruma Analytik GmbH. The substrate temperature was chosen to be 480 °C because higher average V_{OC} values were found at this temperature for Al/ITO-based back contacts.^[16] Directly after CIGSe growth, the samples were objected to a 1 nm NaF post-deposition-treatment by thermal evaporation of NaF at a sample temperature of 450 °C without breaking the vacuum. The solar cells were finished by chemical bath deposition of ≈ 45 nm CdS, 123 nm i-ZnO sputtering, and 240 nm ITO sputtering. Small solar cells of ≈ 10 mm² area are defined by chemical etching of the front contact. For this purpose 10% HCl was applied manually to the front surface, locally removing the ITO/ZnO/CdS layers.

The finished solar cells were characterized using a home-built sun simulator using a halogen lamp. The intensity of the lamp was adjusted by matching the current of a Si reference solar cell to the current anticipated under AM1.5G conditions. EQE measurements were also investigated using a home-built system. Focus-ion-beam (FIB) preparation was carried out using a versa3D from FEI. The layer growth was computed separately for each layer using a self-written Fortran program. 3D finite-difference time-domain (FDTD) simulations were performed using the software package Meep.^[21]

3. Results and Discussion

3.1. Structure Transposition

As a result of the lift-off process, periodic openings in the SiO_2 layer are formed. These openings are surrounded by conical walls. The conical shape of the walls is due to the fact that the diameter of the pillars—consisting of photoresist plus SiO_2 deposit—grows upon prolonged SiO_2 deposition. As the pillars form a shadow for the SiO_2 deposition, the deposited sample surface decreases upon prolonged SiO_2 deposition. For large SiO_2 thickness, the conical walls form a sharp tip. This is the case for the 700 nm SiO_2 thickness in **Figure 2**. Having achieved these SiO_2 openings after lift-off, conformal coverage of the structured back contact would lead to a transposition of the structure to the successively deposited layers. In the lower row of **Figure 2**, SEM cross-sections of complete solar cells are shown. After Al and ITO deposition, the structure height appears to be transposed—meaning that there is no change in structure height and the structure is replicated. This is no longer the case for the CIGSe deposition. Here, the mobility of the deposited species on

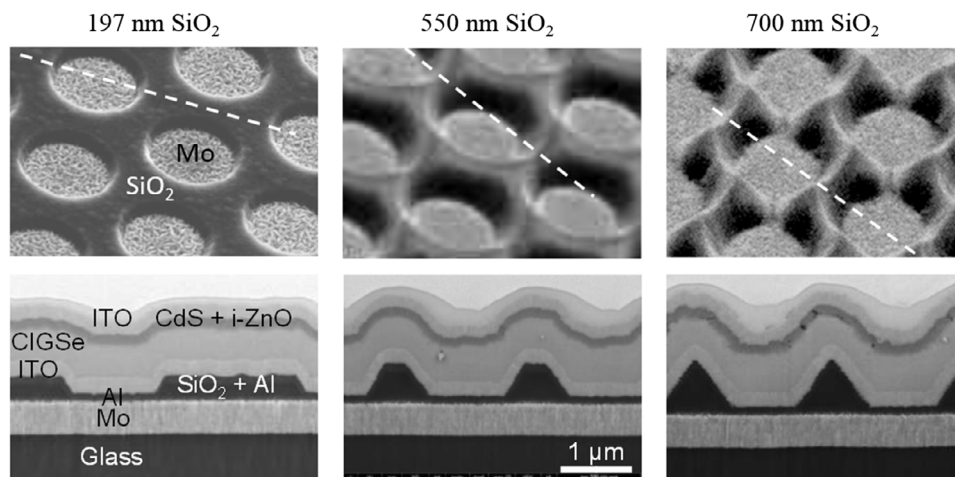


Figure 2. (Top) SEM images of structured SiO_2 layers on a molybdenum back contact for structure heights of 197, 550, and 700 nm. Dashed lines give the orientation of the cross-sections below. (Bottom) SEM images (tilt angle 52°) of FIB prepared cross-sections of the complete structures comprising molybdenum, SiO_2 , Al, ITO, CIGSe, CdS + i-ZnO, ITO. (The specimens were covered in addition by platinum to preserve the top layer from preferred ion etching.) Aluminum and SiO_2 appear with the same shade of gray and cannot be discriminated.

the growth surface may limit the structure transposition to some extent. For low SiO_2 thickness, conformal coverage is greatly achieved; the largest structure height of 700 nm shows a smoothening effect: the structure height of the CIGSe layer is less than of the Al back contact. Surface smoothening can be understood considering adatom surface diffusion^[22] and re-evaporation.^[23] The smoothening has to be considered in optical simulations. Nevertheless, a larger angle of the front interfaces is achieved with respect to the flat sample surface using higher SiO_2 structures. Therefore, incoming light will be scattered in larger angles. We note that the achieved structure is the geometric negative of the pillar structure in ref. [19] producing the same structure height.

The 3D structure of the samples was reconstructed using a self-written computer program with the following model. A sketch of the working principle of the model can be seen in Figure S1, Supporting Information. Two different growth modes were implemented. First, a growth purely in the normal direction of the flat substrate, and second, a growth in the normal direction of the inclined sample surface. In the following, these two growth modes will be denoted as vertical growth and normal growth. The growth of each material layer was described by a mixed growth mode of the two elementary growth modes. The nature of the growth progress can be tuned to mimic the real layer growth by manipulating the portions of the two elementary growth processes used in the calculation. The algorithm for this is the following: the two growth modes were applied in sequence, growing a larger number of sub-layers thinner than the targeted material layer. The resulting thickness of the newly modeled sub-layer is d_{normal} for normal growth and d_{vertical} for vertical growth. The fraction between these two quantities is defined by $\beta = d_{\text{normal}} / (d_{\text{normal}} + d_{\text{vertical}})$. The growth algorithm for each material layer is terminated when the total volume of the material matches the volume measured on the flat reference.

Using the SEM pictures, values for β were extracted for each material by visual comparison. A value of $\beta = 0.5$ was extracted

for CIGS and a value of $\beta = 0.3$ was determined for ZnO, both ITO layers, and Al. It must be noted that the determination for Al is especially error-prone due to its small thickness. No value could be extracted for CdS because the layer was difficult to identify in the SEM cross-sections. This also increases the uncertainty for the determination of β for both CIGSe and ZnO. Overall, a good match of the grown layers and the calculated ones could be achieved. Figure 1 is created from the calculated 3D structure for the solar cell with a 550 nm structure height. Sever et al. developed a calculation model for the layer growth on structured surfaces and used it for a thin-film Si solar cell.^[24] The calculation strategy using the two elementary growth modes connected by a parameter basically is identical to the one used here. Therefore, it is possible to compare the values, although the computational representation of the layers differs from the one used here. A value of $\beta = 0.2$ was found for ZnO and $\beta = 0.3$ for Si. Kovacic et al. applied this model onto a CIGSe absorber and obtained a value of $\beta = 0.3$ for CIGSe.^[20] Two remarks have to be made regarding the determined value for the CIGSe in our work. First, the CIGSe top interface has an additional random structure caused by the crystal size which makes it difficult to determine a precise value for β . An absolute error for β of 0.1 is therefore estimated. Second, the exact growth of the CIGSe is possibly process dependent, e.g., the process temperature affects atom diffusion and crystal size during the deposition process.

3.2. Solar Cell Performance

Figure 3 shows the solar cell parameters for both sample sets. Only the values of the best solar cell for each sample are shown. The results for a 700 nm structure are omitted, due to strong shunting of this sample. Because of this observation, this sample thickness was not repeated in sample set 2. This shunting could be caused by pinholes in the CIGSe layer of this structure. A possible cause could be a cracking of the CIGSe layer at the sharp top edge of these samples caused by mechanical stress through

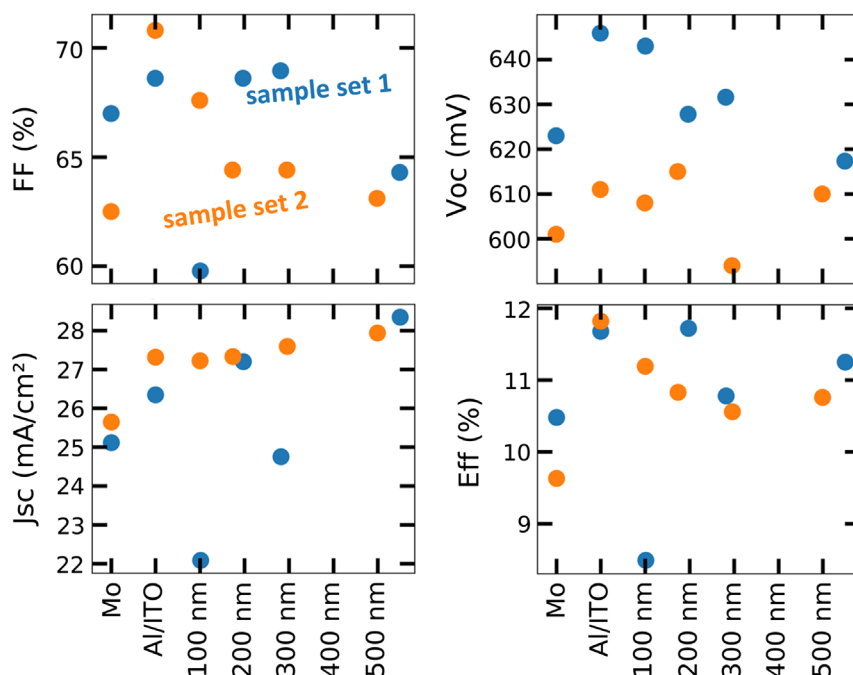


Figure 3. Solar cell parameters of reference sample with Mo back contact, a sample with flat Al/ITO back contact, and structured back contacts with different SiO₂ layer thicknesses for sample sets 1 and 2.

different thermal expansion coefficients of the different materials. However, no such thing was observable from SEM cross-sections.

The FF and V_{oc} values are obtained from J - V measurements. The J_{sc} values are calculated from the EQE curves using the tabulated AM1.5G spectrum. Samples of the sample set 1, in general, show a higher V_{oc} than the samples of the second set. This could be explained by the higher GGI of set 1 or by a better absorber quality. The different GGI gradients as determined by GDOES measurements are shown in Figure S2, Supporting Information. The samples with Al/ITO back contact for most samples show a higher V_{oc} compared with the respective Mo reference. A similar result has been reported in ref. [16], although there the V_{oc} difference was more pronounced. Representative J - V curves are shown in Figure S3, Supporting Information. The shunt resistance determined from the dark J - V curves is above 20 k Ω cm² for all solar cells. Despite this high shunt resistance, a small slope can be seen in the illuminated J - V -curves for 0 V. This indicates problems with carrier collection. A relatively strong crossover can be seen when comparing the dark with the illuminated case. Those effects are visible independent of the used back contact. No trend can be seen for both V_{oc} and the FF when comparing different structure heights.

Regarding J_{sc} , however, a clear trend is visible: the flat Al/ITO samples show an increased J_{sc} of 1.2 and 1.7 mA cm⁻² compared with the Mo sample. In combination with the structured back contact, J_{sc} further increases. This gain increases with increasing structure height. For the 500 nm structures, a total gain of 3.2 and 2.3 mA cm⁻² is achieved compared with their corresponding Mo references. Two outliers from this trend can be seen in sample set 1. By optical inspection, the 101 nm sample appears to exhibit an incomplete lift-off of the photoresist

pillars. Its poor FF and J_{sc} may be explained by photoresist remainings. A similar problem could also explain the poor performance of the 282 nm sample of sample set 1.

The overall efficiency is not increased by the structuring process. Almost all structured solar cells display a decreased efficiency compared to their corresponding flat reference with Al/ITO back contact. The increased J_{sc} caused by structuring is offset by losses in the other PV-parameters. The sample number is, however, too low to conclusively state if the losses in FF and V_{oc} are systematic or if they are caused by the additional handling involved compared with their flat references. The comparison of the flat substrates shows an absolute increase in efficiency of 1.2% for sample set 1 and 2.2% for sample set 2 when comparing the Al/ITO back contact with the corresponding Mo reference. The Al/ITO reference cell of sample set 2 shows the highest efficiency of 11.8%.

Figure 4 shows the measured EQE curves for both sample sets. A solar cell with Mo back contact and the same window structure but with a 2.8 μ m absorber is also given for comparison. Experimental details of the sample preparation for this specific sample are given in the Supporting Information. The unstructured solar cells with Al/ITO rear contact show a distinct peak at \approx 900 nm. This peak is due to an increased light absorption within the absorber layer caused by interference of light entering the solar cell with light reflected at the back contact. The 900 nm peak disappears with increasing structuring height. A second peak is visible for the flat sample of set 2 at 820 nm. The curves for the 101 and 282 nm samples of set 1 both show a decreased EQE over the full spectra (the complete data set is given in Figure S4, Supporting Information). This could hint to electrical problems caused by an incomplete lift-off. For wavelengths above 900 nm, an increase in the EQE is visible with

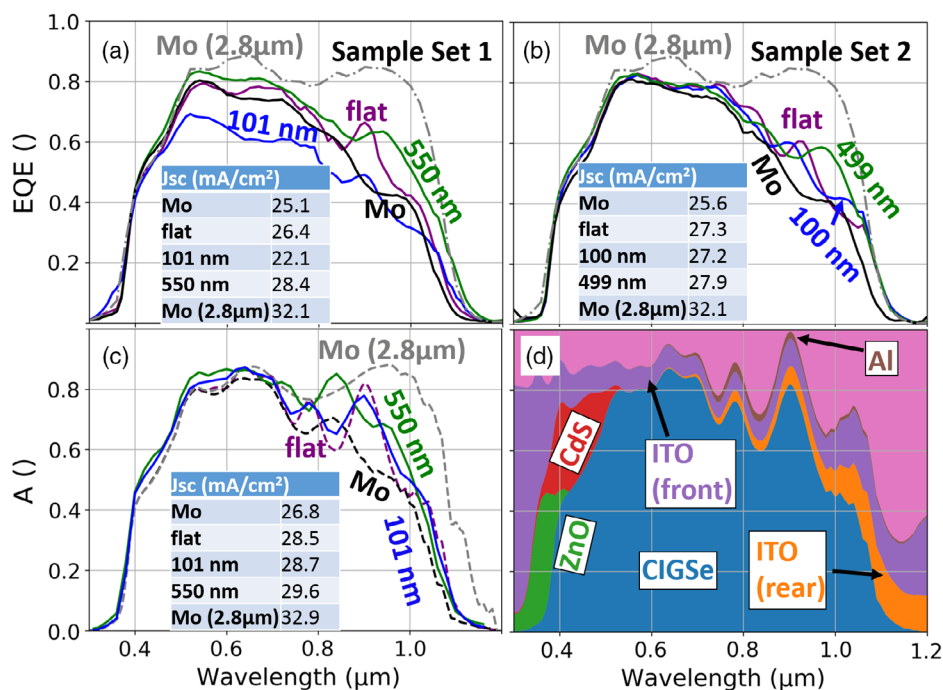


Figure 4. EQE of solar cells with different back contacts for a) sample set 1 and b) sample set 2. An additional CIGSe solar cell with a 2.8 μm absorber and a Mo back contact is shown in both figures for comparison. c) Calculated absorption within the CIGSe layer of a complete solar cell. The dashed lines are calculated using the transfer-matrix-method for an unstructured sample with an Al/ITO back contact (purple), a Mo back contact (black), and a solar cell with Mo back contact with a 2.8 μm absorber (gray). The other curves are from FDTD calculations for the structural dimensions of sample set 1. d) Calculated relative absorption within the separate solar cell layers for an unstructured solar cell with Al/ITO back contact. (The complete EQE measurements and simulations can be found in the Figure S1, Supporting Information).

increasing structure height. This trend is better visible for sample set 2. A small increase in the EQE with increasing structure height is also visible for shorter wavelengths around 600 nm. This could be caused by reduced reflectance at the front interface by the structure. In addition, layer thickness variation of the CdS between different samples can cause a difference for short wavelengths. The best structure reaches about 88% of the J_{SC} value of the given 2.8 μm absorber thickness reference. The band gap of the Al/ITO-based solar cells appears to be lower in comparison to the Mo-based samples. As shown later in the next section, these differences can be explained by optical simulations. The EQE curves of sample set 1 show overall more variation over the whole spectral range. These differences could be explained by a partial unsuccessful lift-off process which is related to the failure of the 101 nm structure. The results of set 2 are therefore probably more representative for the actual influence of the structures on the EQE.

The gain in J_{SC} due to the combination of reflectance and scattering is slightly below the gain in ref. [19], however there, the CIGSe thickness was only 390 nm. This proves the working principle of integration of optical scattering and reflectance in a thin-film solar cell.

3.3. Optical Simulations

For the FDTD simulations, structure models based on sample set 1 were constructed according to the method described in

Section 3.1. The GGI profile extracted from GDOES measurements given in Figure S2, Supporting Information, was implemented in the simulations. For 1D and 3D simulations, the GGI gradient was implemented by dividing the CIGS layer into sub-layers with different GGI according to the GGI gradient. The optical data for an arbitrary GGI value was interpolated from the optical properties found in ref. [25]. The optical coefficients were extracted for both ITO layers as described in ref. [16]. The optical data for the other layers are taken from the literature.^[25–27] The local absorption was calculated for the two polarization directions in x and y direction (the x - and y -axis are defined in Figure 1). The overall absorption was calculated by summing up the local absorptions of the two polarizations. In general, the difference in global absorption in the CIGSe layer for the two polarizations was found to be very small (<0.01%) for all wavelengths. The calculated wavelength-dependent absorption within the CIGSe layer is plotted in Figure 4c. Reference curves were calculated in 1D using the transfer-matrix-method for the unstructured solar cell with Al/ITO back contact as well as for two solar cells with Mo back contact having an absorber thickness of 0.6 and 2.8 μm. These are also given in Figure 4c. The overall shapes of the calculated absorption curves are in close agreement to the corresponding EQE spectra, with the exception of a peak at 820 nm, which is visible for the 550 nm structure in simulations but does not appear in the experiment. This peak might be visible in the 499 nm structure of sample set 2. The previously mentioned apparent difference between the band gaps of samples with Mo back contact in comparison to samples with Al/ITO

back contact is also visible in the simulations. This difference can, therefore, be explained by an increased absorption for the Al/ITO back-contact samples in comparison to the Mo back-contact samples. The peaks are generally more pronounced in the simulations than in the experiment, with EQE values generally lower than the calculated absorption at the peak positions. This can be explained to some extent by the additional random structure caused by the crystal structure of the layers. This structure will apply some additional random scattering and therefore reduce the sharpness of interference peaks. 2D FDTD simulations have been performed additionally to estimate the influence of this surface roughness, which is not included in the other simulations. The layer interfaces were directly extracted from SEM cross-sections. A constant GGI of 0.37 was used for simplicity. The results can be seen in Figure S5, Supporting Information. The reduced peak height in the experiment can only be explained to a smaller degree by surface roughness caused by the crystal size of the layer. The rest of the difference could be related to recombination losses including back-contact recombination losses. In addition, some discrepancies can be seen at around 620 nm with lower EQE values than for the calculated absorption. Theoretically, the overall absorption of all samples should be similar to the 2.8 μm sample in this range. Most of the absorption will happen near the front interface in this wavelength range. Those losses could be therefore related to bulk recombination and recombination within the p–n junction. Further experiments are necessary to understand the electrical losses. In particular, the back-contact recombination velocity for the Al/ITO back contact needs to be determined. The J_{SC} values derived from the EQE are lower by 1.7 mA cm^{-2} for the Mo sample, 2.1 mA cm^{-2} for the Al/ITO sample, and 1.2 mA cm^{-2} for the 550 nm sample compared with the obtained J_{SC} values. Those differences are caused by electrical losses as well as by errors of the simulation caused, for example, by the usage of tabulated CIGSe material properties which may differ from the material properties of the CIGSe used in the experiment. In addition, the values are probably underestimated to some degree by the reduced reflectance through the front surface structuring as seen in Figure S5, Supporting Information.

In summary, the simulation show some additional absorption for shorter wavelength when the SiO_2 structures are added, which are probably related to a decreased front-side reflectivity.

This effect can however not be observed in the EQE results of sample set 2. Therefore, this effect may be overemphasized by the simulation because the sample roughness caused by the crystal size is not considered. This roughness for itself already leads to a reduced reflectance as can be seen in Figure S5, Supporting Information. Most of the experimental gains are seen for longer wavelengths. Therefore, it is likely that a light-path enhancement by scattering is the main cause for the increased short-circuit current by the structure. Compared to a simulated solar cell with 2.8 μm CIGSe layer thickness, 88% of the current density can be achieved with the integrated structured back reflector using 550 nm structure height.

Figure 5a,b shows the local absorption for a solar cell with a 550 nm structure height at a wavelength of 940 nm. The respective plot for the unstructured sample is shown in Figure 5c for comparison. Locally increased absorption caused by interference is visible in the unstructured case. This local absorption is enhanced for the structured case by additional local maxima in the heights of the structure. On the other hand, in the valley, the CIGSe layer exhibits a decreased absorption. Both observations can be explained by scattering of light at the front interface of the structure. Light is scattered from the “valley-region” to the height region. The additional path length through the CIGSe layer caused by the increased angles to the surface normal may already explain the increase in absorption. The portion of the front interface which is curved instead of flat increases with increasing structure height. Therefore, this scattering effect is more pronounced for higher structures. In addition, a smaller region of increased absorption is found in the center of the valley. This local field enhancement is probably caused by light coming directly from the front interface, interacting with light reflected at the conical walls. Overall, this inhomogeneous absorption can lead to regions of the solar cell operating under different illumination conditions. This could have a negative influence on the solar cell parameter. The significance of this is however unclear.

Figure 4d shows the absorption within the different solar cell layers. There are two strong absorption losses related to the non-optimized ITO used in our laboratory. Parasitic absorption occurs in the front ITO for a wide wavelength range. In addition, parasitic absorption occurs within the rear ITO at long wavelengths. This limits the possible gain achievable through the

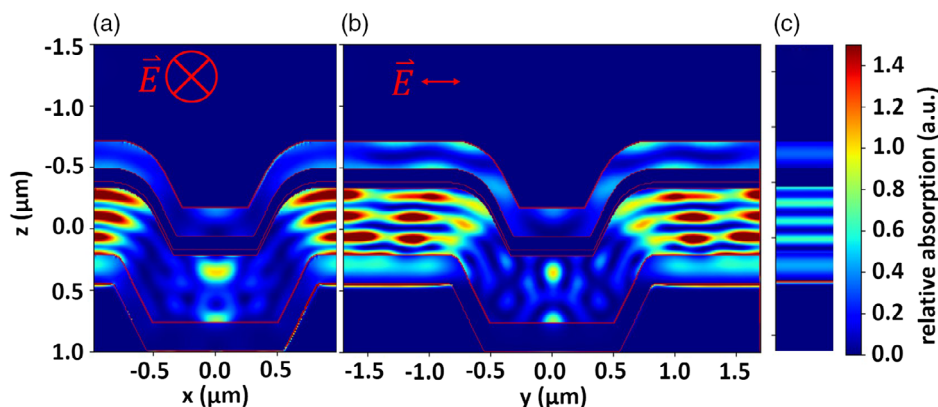


Figure 5. a,b) Calculated local absorption within a solar cell corresponding to the 550 nm structure height sample from sample set 1. The used axes are shown in Figure 1. c) The same data calculated for a flat solar cell with the same layer thicknesses. All pictures share the same color scale, which shows the local absorption within a volume element in arbitrary units.

structuring and could be mitigated by improved material properties and parameters. The relative parasitic absorption of the incoming solar energy within the rear ITO layer, for energies below the bandgap of the CIGSe, was calculated to 3.8% in the flat case, 3.8% for the 101 nm structure, and 4.2% for the 550 nm structure. As experimentally shown in ref. [16], a decrease in the ITO rear thickness from 200 to 100 nm leads to an increased J_{SC} of 0.5 mA cm^{-2} already in the unstructured case.

The simulations of Kovacic et al. on 2D sine-like structures with highly reflective back contact but without parasitic absorption in the rear oxide layer showed the highest increase in J_{SC} for a pitch of $0.8 \mu\text{m}$ and 300 nm structure height.^[20] This suggests that smaller pitches than the here used $1.96 \mu\text{m}$ may lead to higher J_{SC} values. However, absorption effects in the diffusion barrier material ITO layer need to be considered, which may also influence the optimum structure. This optimal structure must confine the light inside the CIGSe without increasing the parasitic ITO absorption.

4. Conclusions

CIGSe solar cells with Al/ITO back reflector were successfully prepared on a nanostructured substrate. Compared with the Mo reference cell, an increase in J_{SC} up to 3.2 mA cm^{-2} was obtained by combining both the Al/ITO back contact and the rear nanostructuring. The I - V curves show further, that the average V_{oc} is increased by $\approx 20 \text{ mV}$ when an Al/ITO back contact is used instead of the standard Mo back contact for 600 nm thick CIGSe. The growth of the solar cell layers was studied using SEM cross-sections. The overall structure is only partly transposed to the front side of the solar cell. A simple model was used to reconstruct the layers in 3D. 3D optical simulations were used to calculate the changes in absorption within the CIGSe layer. A good match was found between simulations and experimental EQE curves. The simulations reveal that further optical gain can be achieved by reduced parasitic absorption within the ITO layers. Compared to a $2.8 \mu\text{m}$ CIGSe solar cell with Mo rear contact and the same window layers, the best structure reaches according to experiment already 88% of the J_{SC} value. It is expected that this value can be further improved by both reducing the ITO diffusion barrier thickness and through optimization of the structural dimension of the rear nanostructure.

Supporting Information

Supporting Information is available from the Wiley Online Library or from the author.

Acknowledgements

The authors gratefully acknowledge the funding through the BMBF project StrukturSolarII (Nr: 03EK3570B). Open-access funding enabled and organized by Projekt DEAL.

Conflict of Interest

The authors declare no conflict of interest.

Keywords

alternative back contacts, layer growth, optical simulations, ultrathin CIGSe solar cells

Received: June 10, 2020

Revised: July 28, 2020

Published online: August 13, 2020

- [1] L. M. Mansfield, A. Kanevce, S. P. Harvey, K. Bowers, C. Beall, S. Glynn, I. L. Repins, *Prog. Photovoltaics* **2018**, *26*, 949.
- [2] R. Scheer, H.-W. Schock, *Chalcogenide Photovoltaics – Physics, Technologies, and Thin Film Devices*, Wiley VCH, Weinheim **2011**.
- [3] J. Goffard, C. Colin, F. Mollica, A. Cattoni, C. Sauvan, P. Lalanne, J. Guillemoles, N. Naghavi, S. Collin, *IEEE J. Photovoltaics* **2017**, *7*, 1433.
- [4] J. Krc, M. Sever, A. Campa, Z. Lokar, B. Lipovsek, M. Topic, *Thin Solid Films* **2017**, *633*, 193.
- [5] E. Jarzembowski, F. Syrowatka, K. Kaufmann, W. Fränzel, T. Hölscher, R. Scheer, *Appl. Phys. Lett.* **2015**, *107*, 051601.
- [6] B. Vermang, J. T. Wätjen, V. Fjällström, F. Rostvall, M. Edoff, R. Gunnarsson, I. Pilch, U. Helmersson, R. Kotipalli, F. Henry, D. Flandre, *Thin Solid Films* **2014**, *582*, 300.
- [7] G. Birant, J. D. Wild, M. Meuris, J. Poortmans, B. Vermang, *Appl. Sci.* **2019**, *9*, 677.
- [8] E. Jarzembowski, B. Fuhrmann, H. Leipner, W. Fränzel, R. Scheer, *Thin Solid Films* **2017**, *633*, 61.
- [9] J. Malmström, S. Schleussner, L. Stolt, *Appl. Phys. Lett.* **2004**, *85*, 2634.
- [10] Z. J. Li-Kao, N. Naghavi, F. Erfurth, J. F. Guillemoles, I. Gérard, A. Etcheberry, J. L. Pelouard, S. Collin, G. Voorwinden, D. Lincot, *Prog. Photovoltaics* **2012**, *20*, 582.
- [11] K. Orgassa, H. W. Schock, J. H. Werner, *Thin Solid Films* **2003**, *387*, 431.
- [12] B. Bissig, R. Carron, L. Greuter, S. Nishiwaki, E. Avancini, C. Andres, T. Feurer, S. Buechler, A. Tiwari, *Prog. Photocatal. Res. Appl.* **2018**, *26*, 894.
- [13] T. Nakada, Y. Hirabayashi, T. Tokado, D. Ohmori, T. Mise, *Solar Energy* **2004**, *77*, 739.
- [14] C. M. Liu, W. L. Liu, W. J. Chen, S. H. Hsieh, T. K. Tsai, L. C. Yang, *J. Electrochem. Soc.* **2005**, *152*, 234.
- [15] L. Gouillart, A. Cattoni, J. Goffard, F. Donsanti, G. Patriarche, M. Jubault, N. Naghavi, S. Collin, *Thin Solid Films* **2019**, *672*, 1.
- [16] T. Schneider, R. Scheer, in *Proc. 36th European Photovoltaic Solar Energy Conf.*, WIP Wirtschaft und Infrastruktur GmbH & Co Planungs KG, Marseille, France **2019**, p. 684.
- [17] J. Keller, W.-C. Chen, L. Riekehr, T. Kubart, T. Törndahl, M. Edoff, *Prog. Photovoltaics* **2018**, *26*, 846.
- [18] E. Yablonovitch, *J. Opt. Soc. Am.* **1982**, *72*, 899.
- [19] G. Yin, M. W. Knight, M.-C. van Lare, M. M. Solà Garcia, A. Polman, M. Schmid, *Adv. Opt. Mat.*, **2017**, *5*, 1600637.
- [20] M. Kovacic, J. Krc, B. Lipovsek, W.-C. Chen, M. Edoff, P. J. Bolt, J. van Deelen, M. Zhukova, J. Lontchi, D. Flandre, P. Salomé, M. Topic, in *36th European Photovoltaic Solar Energy Conf.*, **2019**, p. 654.
- [21] A. Oskooi, D. Roundy, M. Ibanescu, P. Bermel, J. D. Joannopoulos, S. G. Johnson, *Comput. Phys. Commun.* **2010**, *181*, 687.
- [22] T. B. T. To, V. B. de Sousa, F. D. A. Aarão Reis, *Phys. A* **2018**, *511*, 240.
- [23] T. Karabacak, *J. Nanophoton.* **2011**, *5*, 052501.
- [24] M. Sever, J. Krč, M. Topič, *Thin Solid Films* **2014**, *573*, 176.
- [25] G. Yin, Ph.D Thesis, Technical University of Berlin, **2015**.
- [26] K. M. McPeak, S. V. Jayanti, S. J. P. Kress, S. Meyer, S. Iotti, A. Rossinelli, D. J. Norris, *ACS hotonics*, **2015**, *2*, 326.
- [27] K. Orgassa, *Coherent Optical Analysis Of The ZnO/Cds/Cu(In,Ga)Se2 Thin Film Solar Cell*, Shaker Verlag, Aachen **2004**.